

## Activated Carbon Electrode Made From Coconut Husk Waste For Supercapacitor Application

E. Taer<sup>1,\*</sup>, R. Taslim<sup>2</sup>, A. W. Putri<sup>1</sup>, A. Apriwandi<sup>1</sup>, and A. Agustino<sup>1</sup>

<sup>1</sup> Department of Physics, University of Riau, 28293 Simpang Baru, Riau, Indonesia

<sup>2</sup> Departement of Industrial Engineering, State Islamic University of Sultan Syarif Kasim, 28293 Simpang Baru, Riau, Indonesia.

\*E-mail: [erman.taer@lecturer.unri.ac.id](mailto:erman.taer@lecturer.unri.ac.id)

Received: 25 June 2018 / Accepted: 16 September 2018 / Published: 5 November 2018

---

Activated carbon electrode was produced from coconut husk by using a combination of physical and chemical activation methods. Potassium hydroxide (KOH) was used as an activator during chemical activation while carbon dioxide gas (CO<sub>2</sub>) was used as an activator during physical activation in range of 750-900 °C. The physical properties of the carbon electrode was characterized by determining the density, thermogravimetry analysis, degree of microcrystallinity, surface morphology, chemical components and surface area. The crystallinity, surface morphology, and chemical content of the carbon electrode was determined by X-ray Diffraction, Scanning Electron Microscopy, and Energy Dispersive Spectroscopy. The electrochemical properties of the electrodes were reviewed by using a two-electrode system while the capacitive properties of the electrodes was determined using cyclic voltammetry. The high temperature of the physical activation resulted in the complete evaporation of volatile biomass, thereby increasing the carbon content and surface area (from 823 m<sup>2</sup> g<sup>-1</sup> to 1033.20 m<sup>2</sup> g<sup>-1</sup>) of the electrodes. In addition, the increase in the physical activation temperature shows the presence of nanofibers in the morphology of the surface electrode. The electrochemical properties of the electrode showed excellent capacitive properties of a supercapacitor cell, with a very high specific capacitance of 184 F g<sup>-1</sup>.

---

**Keywords:** physical activation, coconut husk, activated carbon electrode, supercapacitor

### 1. INTRODUCTION

The coconut (*Cocos nucifera L.*) is one of the largest cultivated plants in Indonesia. Indonesia is the world's largest producer of coconut. In the year 2016, coconut production in Indonesia reached 18.3 million tons [1]. Almost every part of a coconut plant can be used for diverse purposes. For instance, coconut wood is used as building materials [2], coconut leaves are used for decoration and

food packaging, coconut sticks are used as broomsticks [3], coconut water and coconut husk can be used as fuel [4] and nata decoco [5], and coconut fibers are used as ropes [6]. The biggest coconut waste is shell and husk [7]. The advent of technology has ushered in the increased utilization of coconut shell and husk. Shells and husk have different properties, the shell has a hard and a more dense structure while the husk has a softer structure composed of microfibers. This difference in physical properties contributes to the difference in the chemical properties of carbon when shells and husks are used to produce electrodes in a storage device.

The coconut shell produces carbon with a relatively low internal resistance and good electrical conductivity properties. Several reports have been published on the use of various methods to improve the pore properties of carbon coconut shell electrodes with a combination of superior ion and electron transfer properties. Some studies have documented the use of coconut shells for the storage of energy [8]. Carbon electrodes are produced using phosphoric acid ( $\text{H}_3\text{PO}_4$ ) activation with the rapid cooling method. The conduction of electrochemical test showed that the carbon electrode produced from using this method exhibited an excellent doublelayer capacitance performance, with a specific capacitance of  $101.68 \text{ F g}^{-1}$  [8]. Coconut shells are used in the production of flexible carbon activated electrode for supercapacitor application. The extensive surface and optimum capacitance obtained from this flexible carbon activated electrode is  $194.429 \text{ m}^2 \text{ g}^{-1}$  and  $10.55 \text{ F g}^{-1}$  [9]. On the other hand, some researchers have described the superiority of micro and nanofibers in the shallow pores of coconut husks resulting in a low ion diffusion relaxation time to produce high power on the supercapacitor device. The study of the utilization of coconut husk as the material of carbon electrode for supercapacitor still lower relatively compared of coconut shell. Yin *et al.* (2016) documented that the preparation carbon electrode from coconut husk for a supercapacitor cell resulted in the production of a carbon electrode with a specific capacitance of  $266 \text{ F g}^{-1}$  [10]. Also, the study conducted by Yin *et al.* (2016) documented that the supercapacitor electrodes made from coconut husk contains hollow fiber cells that facilitates the effective diffusion of ions to the electrodes.

Many studies have documented the use of potassium hydroxide (KOH) activators and adhesive materials in the production of carbon electrode from coconut shells. Thus, this study investigated the use of a combination of the chemical activation method and physical activation process (without the use of additional adhesive materials in pellet or monolithic form) in the production of carbon electrodes for supercapacitor applications.

## 2. EXPERIMENTAL DETAILS

Coconut husks were used as the basic raw material for the production of carbon electrodes. The coconut husks were broken down into fibers and cut into lengths of 2-5 cm to facilitate the heating process. The coconut husks were then sun-dried and oven-dried for 48 hours at  $110 \text{ }^\circ\text{C}$ . The dried sample was pre-carbonized at a temperature of  $250 \text{ }^\circ\text{C}$  for 2 hours; this process converted the dried sample into a powdered substance. The sample was then converted from powder to pellet by using the method as previously reported [11]. Chemical activation of coconut husk carbon was carried out using KOH as an activator at low concentration [12], the mass ratio of carbon to KOH was 1: 1/4. The

pyrolysis process (which includes carbonization and physical activation) was carried out in a one stage integrated system [13]. The pyrolysis process began at low temperature using nitrogen ( $N_2$ ) gas at a temperature of 600 °C. This step was followed by the physical activation of the carbon using carbon dioxide ( $CO_2$ ) gas for 2.5 hours. The varying range of temperatures used in this study include 750 °C, 800 °C, 850 °C, and 900 °C. The sample codes used in this study include ACC-750, ACC-800, ACC-850, and ACC-900; the full meaning of ACC is Activated Carbon Coconut. All electrode samples were polished and washed until the pH of the wash water became neutral [pH=7]. The preparation process of the activated carbon electrodes from coconut husk is shown in Figure 1.

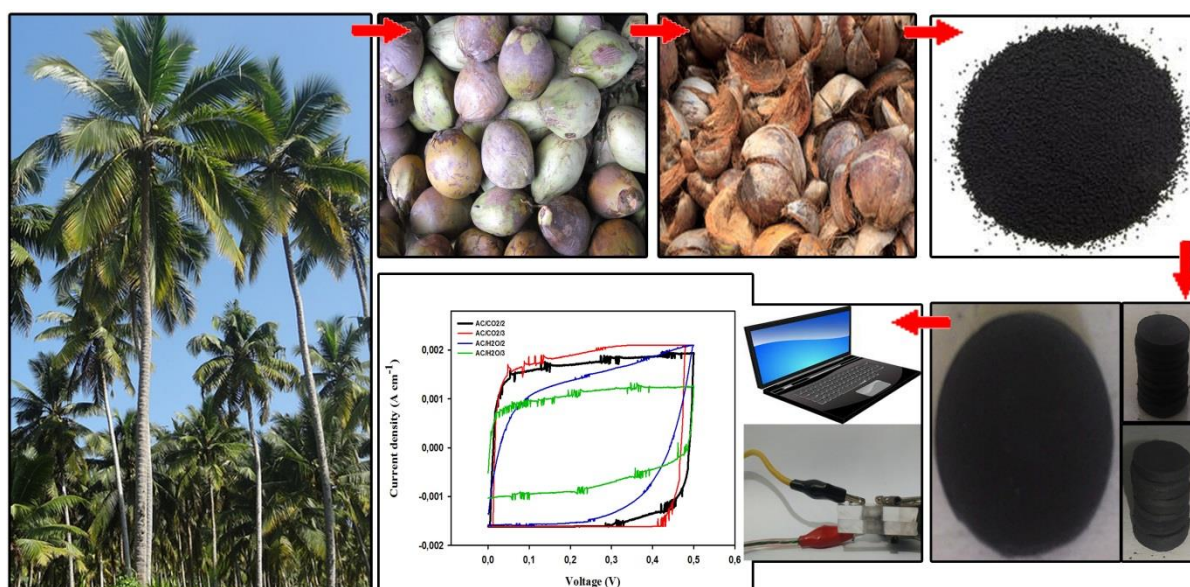


**Figure 1.** Preparation process of the activated carbon electrodes from coconut husk

The physical properties of the carbon electrode was characterized by determining the i.e density, thermogravimetry analysis, degree of microcrystallinity, surface morphology, chemical components and surface area. The density was evaluated by measuring the mass and dimensions of carbon pellets before and after pyrolysis. Thermogravimetry analysis was conducted using the Netzsch derivatograph (STA 449 F1 Jupiter instrument). The crystallinity of the carbon electrode was reviewed by using the X-ray diffraction method (Philip X-Pert Pro PW 3060/10). The surface morphology and chemical content of the carbon electrode were evaluated using Scanning Electron Microscopy and Energy Dispersive Spectroscopy method (SUPRA instrument S-3400N series). The surface area of the carbon electrode was calculated using the standard formula from microcrystalline height data obtained from XRD analysis [14]. The electrochemical properties of the electrodes were reviewed by using a two-electrode system. The supercapacitor cell comprised of carbon electrodes, current collectors, electrolytes and separators. The electrolyte used was 1 M sulfuric acid ( $H_2SO_4$ ) [15] and separator duck egg shell membrane [16]. The cyclic voltammetry method was used to review the capacitive properties of the electrodes. The capacitive properties of the electrodes was tested using the CV UR Rad-Er 5841 instrument that had been calibrated using 1280 solatron device.

### 3. RESULTS AND DISCUSSION

#### 3.1. Density analysis

In physics, the activation temperature using CO<sub>2</sub> gas has a great effect on the density properties. The variation in temperature of physical activation makes the particles of carbon break down more smoothly forming new pores. The extra time of physics activation causes the pores of the cell to increase, resulting in an increase in the diameter and a decrease in density. Table 1 shows the average density ratio of carbon electrode before and after pyrolysis. The table shows an appreciable fall in the density of the carbon electrode. This development is occasioned by the process of carbonization which eliminates other elements competing with carbon, thereby lowering the density of carbon electrode. At this stage, the carbon is not strong enough and requires activation to become stronger leading to the formation of more pores. In the course of physical activation, the carbon is subjected to scraping by the reaction of CO<sub>2</sub> gas on its surface. This process leads to the production of new pores and the development of the pre-existing ones [17, 18]. The temperature of the physical activation that is very high created more vaporized compound in such a way that both the mass and the density of the electrode decrease. The data in Table 1 indicates the highest fall in density which occurred when the activation temperature stood at 900 °C. These conditions made the other elements such as oxygen and hydrogen on the surface of the carbon electrode undergo more evaporation [19] to produce more pores and eventually resulting in the smallest densities.

**Table 1.** Comparison of density before and after pyrolysis

Sample codes	Density	
	Before pyrolysis (cm <sup>3</sup> g <sup>-1</sup> )	After pyrolysis (cm <sup>3</sup> g <sup>-1</sup> )
ACC-750	0.991	0.974
ACC-800	0.998	0.948
ACC-850	0.959	0.823
ACC-900	0.938	0.813

#### 3.2. Analysis of Thermal Property

Thermal stability properties of coconut husk are analyzed using thermogravimetry analysis (TGA) method. The aim of TGA analysis is to determine the highest reduction temperature to be used as a temperature that is resistant to pyrolysis process. The analysis of TGA in this research is represented by two curves, namely Thermal Gravimetry (TG) and Differential Thermal Termographymetry (DTG) curve as illustrated in Figure 2. The TG curve measures the percentage of mass shrinkage as being proportional to temperature whereas the DTG curve determines the reduction in mass or weight per unit time per temperature and thermal stability of a material.

TG and DTG analysis of coconut husk powder sample was carried out using nitrogen pyrolysis gas flowing at the rate of 100 ml per minute and at a temperature range 300 °C -600 °C. The scan rate

temperature of  $10\text{ }^{\circ}\text{C min}^{-1}$  and the weight 6.874 mg of the tested sample were used. The TG curve manifests a decrease in the sample mass which is caused by the decomposition of complex compounds such as lignin, cellulose, and hemicellulose. The TG curve shown in Figure 2 indicates decrease of mass to temperature in 4 stages. The first stage occurs at a temperature of  $93.3\text{ }^{\circ}\text{C}$  with a mass loss of 5.6%. This first decrease shows evaporation of the water content in the sample. The second stage occurs up to temperature of  $244\text{ }^{\circ}\text{C}$  with lost mass as high as 9.37%. Decomposition and evaporation of lignin and hemicellulose compounds were responsible for the decrease. The hemicellulose undergoes decomposition from  $200\text{ }^{\circ}\text{C}$  to  $300\text{ }^{\circ}\text{C}$  while the lignin breaks down from  $160\text{ }^{\circ}\text{C}$  to  $900\text{ }^{\circ}\text{C}$  [20].

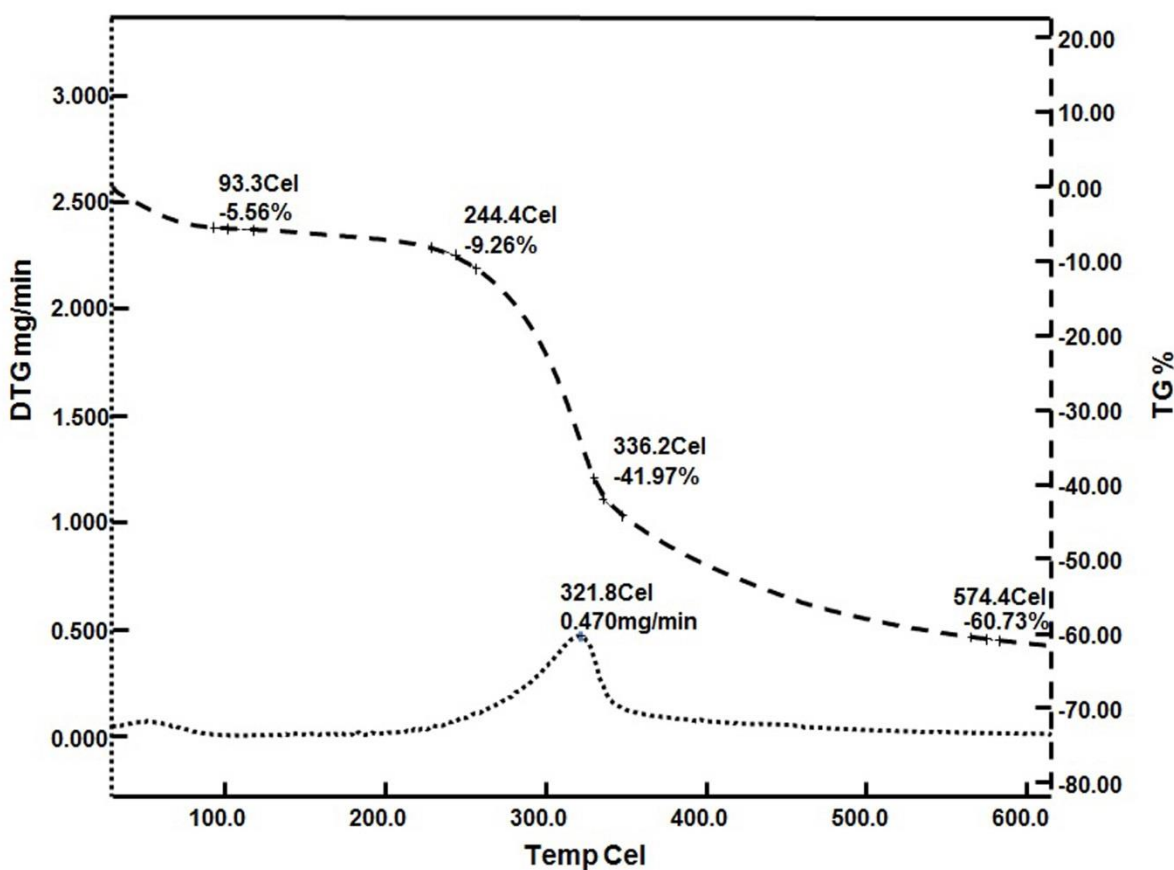


**Figure 2.** DTG/TG curve of carbon coconut husk

The third stage is the highest phase of mass shrinkage reaching 41.97% of the total sample mass. In the third stage, it is shown that all complex compounds such as hemicellulose, cellulose and lignin have decomposed at the same time [21]. Following this case, the mass of the sample still indicated a shrinkage that is at fourth stage in which the sample is still experiencing shrinkage of the mass at a temperature of  $574.4\text{ }^{\circ}\text{C}$ . The reduction in size at this stage is caused by the breakdown of the lignin compound which is still ongoing until it reaches the temperature of  $900\text{ }^{\circ}\text{C}$ . The decomposition of material indicates that the sample has good thermal stability at temperatures above  $600\text{ }^{\circ}\text{C}$ . The DTG curve shows a significant reduction in mass reaching the peak at temperature of  $321.8\text{ }^{\circ}\text{C}$  with a

decomposition rate of  $0.470 \text{ mg min}^{-1}$ . This is influenced by the reduction in size of complex compounds which occur at the same time resulting in a marked shrinkage of mass. This analysis is validated by a previously presented TG analysis which in this temperature range of complex compounds such as hemicellulose, cellulose and lignin decompose simultaneously. Based on the foregoing, it can be rightly concluded that the temperature of  $321.8 \text{ }^\circ\text{C}$  is the thermal resistance for coconut husk biomass. This temperature is used in the pyrolysis process to be held for 1 hour. The holding time of 1 hour is aimed to produce better carbon.

### 3.3. XRD analysis

Figure 3.a shows the XRD curve pattern of active carbon electrode produced from coconut husk. This curve is identical with an amorphous carbon with two widening peaks [11]. The result of X-ray diffractions is used to evaluate microcrystallinity dimensions using Microcal Origin software. Microcrystallinity dimensions such as interlayer spacing, diffraction angle, microcrystallinity height and microcrystallinity width evaluated by using Bragg [22] equation and standard formulas [23, 24, 25, 26] whose values are shown in Table 2.

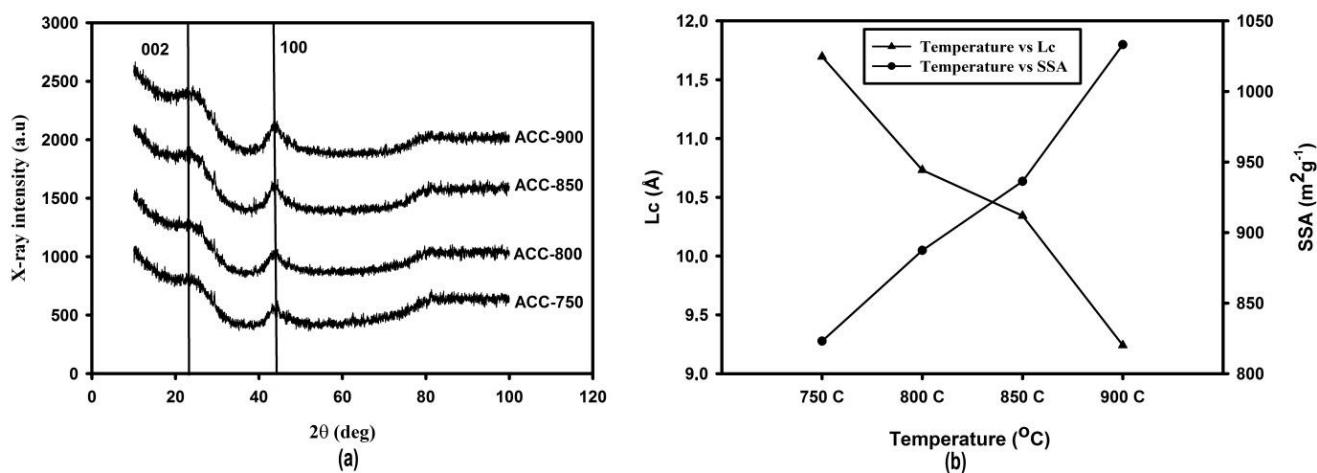


**Figure 3.** a) X-Ray Diffraction curve; b) Relationship of physical activation temperature to SSA and Lc

The data shown in Table 2 shows the microcrystallinity parameters which provide information about the diffraction angle that is the effect of microcrystallinity width ( $L_a$ ) and microcrystallinity height ( $L_c$ ) in the observed sample. Each sample has an amorphous peak at different angle ranges. The ACC-900 sample has the smallest  $L_c$  while for ACC-800, ACC-850 and ACC-900 samples indicated decreasing  $L_c$  value with increasing activation temperature. Significantly, decreasing  $L_c$  was found as high as  $9.241 \text{ \AA}$  in ACC-900 samples which were activated at a temperature of  $900 \text{ }^\circ\text{C}$ . The  $L_c$  can be used as a reference to determine surface area sample. The microcrystallinity height relationship with the microcrystallite graphite and the Specific Surface Area (SSA) in the activated carbon electrode. It is indicate in the empirical formula  $\text{SSA}_{\text{xrd}} = 2/(\rho_{\text{xrd}}L_c)$  where  $\rho_{\text{xrd}}$  represented the XRD density

whose is obtained from  $\rho_{\text{xrd}} = \{d_{002}(\text{graphite}) / d_{002}\} \rho_{(\text{graphite})}$  with values of  $d_{002}(\text{graphite}) = 0.33354$  nm and  $\rho_{(\text{graphite})} = 2.268$  g cm<sup>-3</sup> [14, 27]. The surface area of each sample increases with rising activation temperature. The ACC-900 sample has the highest surface area compared to other samples of 103.20 m<sup>2</sup> g<sup>-1</sup>. The specific Surface Area (SSA) produced in this study is smaller than the specific surface area produced by Yin et al., 2016 with the same biomass of 2898 m<sup>2</sup> g<sup>-1</sup> [10]. This comparison may not be unconnected with the difference in the addition of more KOH. Based on this comparison, it can be concluded that the specific surface area found by using XRD method represents the general surface area of activated carbon electrode made from coconut husk. The relationship between physical activation temperature to surface area and Lc is indicated in the Figure 3.b. The rise in temperature is directly proportional to the surface area but inversely proportional to Lc. This increase in surface area is affected by decreasing Lc.

**Table 2.** Diffraction angle ( $2\theta$ ), interlayer spacing ( $d$ ), microcrystallinity height (Lc) and microcrystallinity width (La)

Sample codes	$2\theta_{002}(^{\circ})$	$2\theta_{100}(^{\circ})$	$d_{002}(\text{\AA})$	$d_{100}(\text{\AA})$	Lc ( $\text{\AA}$ )	La ( $\text{\AA}$ )
ACC-750	24.428	44.019	3.641	2.055	11.696	82.397
ACC-800	24.698	44.448	3.602	2.037	10.732	26.306
ACC-850	24.277	44.724	3.663	2.025	10.344	29.569
ACC-900	24.633	44.175	3.611	2.049	9.241	30.485

### 3.4. Surface morphology analysis

The SEM characterization of electrode samples using magnifications of 5000x and 40000x on ACC-800 and ACC-900 is shown in Figure 4. The SEM image using 5000x magnification shows the presence of an agglomerate of dense particles with small and irregular pores between them that are difficult to measure. The SEM characterization of electrode samples with magnification 40000x on ACC-800 and ACC-900 is shown in Figure 4. In Figure 4a shows that there is a considerable amount of carbon-shaped fiber on the surface of the sample, derived from coconut husk fibers. The length of carbon fiber formed ranged from 616 nm to 818 nm while the diameter of carbon fiber formed ranged from 65 nm to 125 nm. Figure 4.b shows the presence of a finer carbon fiber compared to the ACC-800 sample. The length of the carbon fiber ranged from 259 nm to 597 nm while the diameter of the carbon fiber ranged from 59 nm to 85 nm. These values are smaller compared to the values recorded for the carbon fiber in the ACC-800 sample. This is because the addition of physical activation temperature ceroded the carbon fiber, thereby reducing the fiber diameter. The surface morphological appearance generated in this study is similar to that reported by Yin *et al.*, 2016 [10]. Yin *et al.*, (2016) reported that coconut husk-based carbon fibers are hollow. However, the presence of hollow fibers were not seen clearly in this study. This result difference may be due to the instrument used to characterize the carbon electrode samples. Ideally, the instrument used to observe hollow carbon fibers is TEM with an energy of 200 kV.

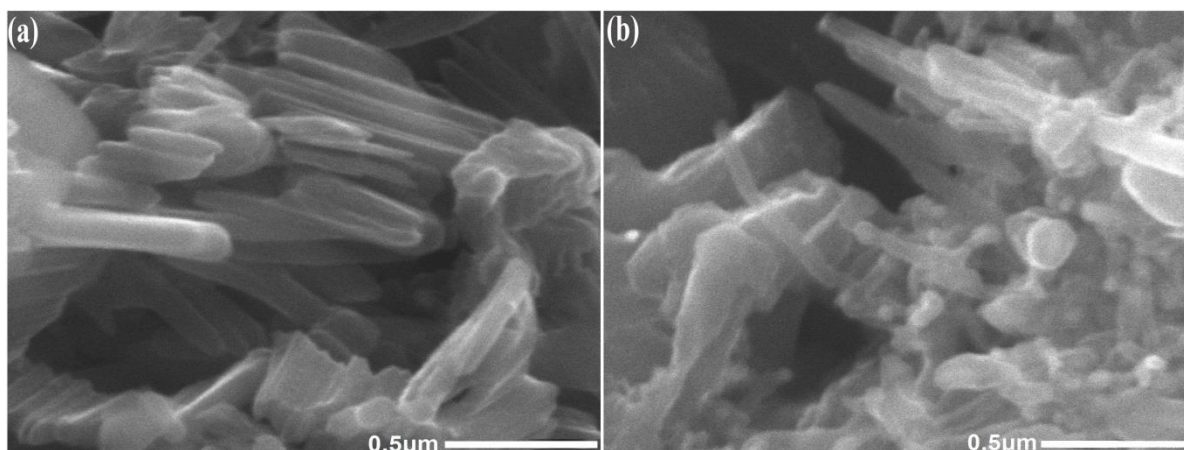


**Figure 4.** SEM images using 40000x magnification for (a) ACC- 800 and (b) ACC- 900

### 3.5. Element content analysis

The element content was characterized by using the X-ray dispersive energy (EDX) method. The EDX analysis showed the level of carbon element purity and other elements present in the coconut husk carbon electrode samples. The results of EDX characterization are presented in Figure 5 for ACC-800 and ACC-900 samples. The result of the EDX analysis revealed that the element content from coconut husk materials (such as Carbon (C), Oxygen (O), Silica (Si) and Potassium (K)) were present. The highest peak was recorded for the carbon element compared to the other elements. This high carbon peak indicates that carbon is the highest elemental content of the electrode sample. The oxygen content is due to the presence of carbon and oxygen bonds at the activation process. The presence of silica elements is due to the presence of biomass materials while the potassium content is due to the utilization of KOH activators (that were not neutralized properly) in the chemical activation process. The percentage composition of each element in the activated carbon electrodes is shown in Table 3. The data in Table 3 indicates that the ACC-800 and ACC-900 samples have the same elemental content of Carbon (C), Oxygen (O), Silica (Si), and Potassium (K). The high percentage of carbon content indicates the effect of high temperature on the physical activation process. Thus, it can be inferred that the temperature used in the physical activation process is the optimum temperature for the preparation of carbon from biomass.

**Table 3.** EDX Data for ACC-800 and ACC-900

Element content	Sample codes			
	AAC-800		ACC-900	
	Wheight (%)	Atom (%)	Wheight (%)	Atom (%)
Carbon	92.66	95.33	93.65	96.32
Oxygen	4.92	3.80	3.52	2.72
Silica	0.86	0.38	0.56	0.25
Potassium	1.56	0.49	2.27	0.72
Totals	100%			

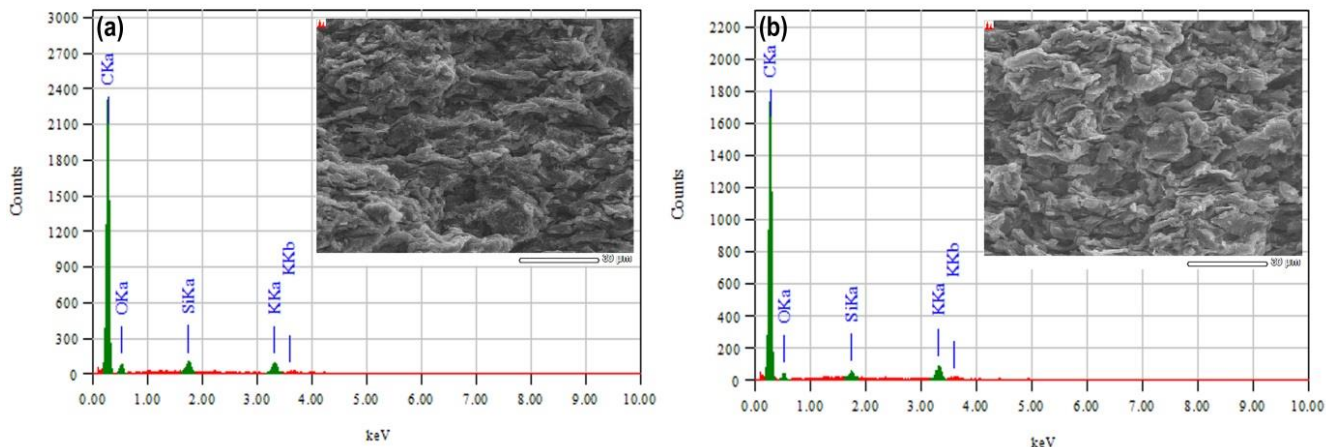


Figure 5. EDS spectra for a) ACC-800; b) ACC-900

3.5. The capacitive property analysis

The electrochemical properties of electrodes for supercapacitors was measured using the cyclic voltammetry (CV) method. The CV curve shows the relationship between voltage and current density (Figure 6). Current density is expressed as the charge current density ( $I_c$ ) and discharge current density ( $I_d$ ).

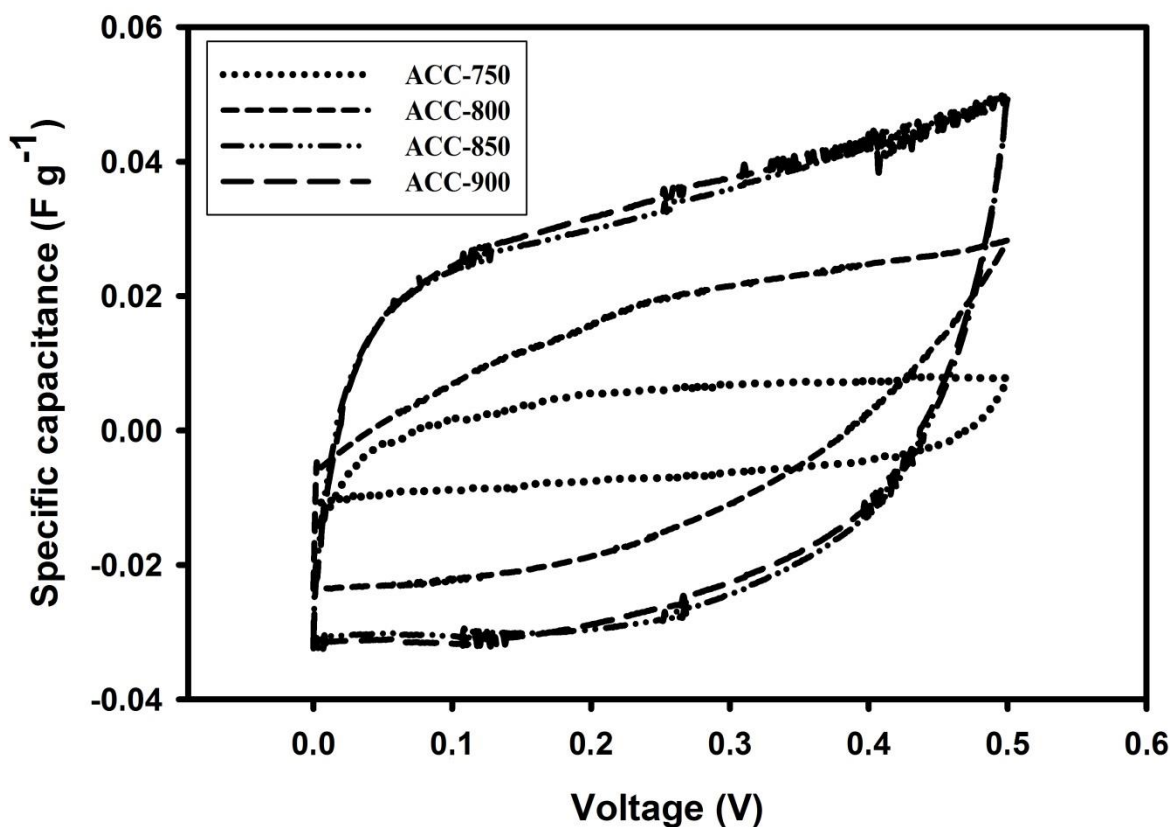


Figure 6. The CV curve for all activated carbon electrodes

The charge current density is the amount of current formed during the process of charging the

ion into the electrode pores at a potential of 0.0–0.5 V while the discharge current density is the current formed at the discharge with the voltage of 0.5–0.0 V [28]. CV measurements were performed at 1 mV s<sup>-1</sup> scan rate; this rate was allow ions to diffuse evenly to the surface area and into the pores of the carbon electrode, thereby improving the capacitance of the supercapacitor [29]. Figure 6 shows the differences area based on the charge and discharge currents in the observed sample. The area of the ACC-750 sample had the lowest value of charge and discharge currents while the areas of the ACC-800, ACC-850, and ACC-900 samples displays increasing the area. There was a significant increase in the area of the current in sample ACC-750 to sample ACC-850 while a relatively small increase was recorded from sample ACC-850 to sample ACC-900. These results show that the temperature activation process affects the area  $I_c$  and  $I_d$  currents. Thus, an increase in the temperature of activation resulted in a wider  $I_c$ - $I_d$  curve.

The current-area curves are directly proportional to the specific capacitance generated by the supercapacitor cells. Thus, it can be inferred that the ACC-900 sample has the highest specific capacitance, followed by ACC-850, ACC-800, and ACC-750 samples. The ACC-900 sample presents a wider curve area; this indicates the greater performance and storage capability of electrochemical energy. The specific capacitance of the cyclic voltammetry analysis can be determined using standard equations.

For all samples of the current of  $I_c$ - $I_d$ , the average mass of the electrode ( $m$ ), and the specific capacitance of the supercapacitor ( $C_{sp}$ ) are shown in Table 4. The lowest specific capacitance of 98 F g<sup>-1</sup> was recorded in the ACC-750 sample while the highest specific capacitance of 184 F g<sup>-1</sup> was recorded in the ACC-900 sample. The conduction of physical activation at a temperature of 750 °C did not result in the complete evaporation of the volatile substances contained in the coconut husk. Hence, there was still a lot of impurity in sample ACC-750. On the other hand, the impurity removal process was more effective in sample ACC 900. This is evident in the difference of the density of both samples: ACC-750 had a density of 0.974 g.cm<sup>-3</sup> while ACC-900 had a density of 0.813 g cm<sup>-3</sup>. The higher physical activation temperature caused the porosity of the samples to increase. This resulted in the perfect diffusion of more ions into the electrode to form a charge pair, which results in the higher capacitance of supercapacitor cells. The ACC-900 sample had the highest specific capacitance; hence, a temperature of 900 °C may be selected as the optimum temperature for the syntesis of carbon electrodes from coconut husk.

**Table 4.** Specific capacitance for all samples

Sample codes	$I_c$ (A m <sup>-2</sup> )	$I_d$ (A m <sup>-2</sup> )	$m$ (g)	$C_{sp}$ (F g <sup>-1</sup> )
ACC-750	0.000368	-0.000425	0.0082	98
ACC-800	0.000950	-0.000750	0.0125	136
ACC-850	0.001233	-0.001070	0.0131	175
ACC-900	0.001329	-0.001015	0.0128	184

**Table 5.** Comparison of specific capacitance (Csp) of electrodes from different biomass.

Biomassa	Csp (F g <sup>-1</sup> )	References
Hemp	144	[32]
Apiaria	177	[33]
Cellulosa acetate	241	[34]
Bamboo powder	218	[35]
Durian Shell	103.6	[36]
Banana Stem	104.2	[37]
Banana peel	206	[38]
Oil palm fruit	150	[39]
Banana Stem	170	[40]
Rubber Wood Sawdust	138	[11]
Coconut husk waste	184	Present study

The specific capacitance obtained in this study is similar to that documented by Yin *et al.*, (2016) [10]. This difference in capacitive properties is influenced by different KOH concentrations. The low KOH concentration maintains the coconut husk carbon powder adhesive properties, thereby resulting in the production of electrodes without the addition of adhesives. In addition, the resulting capacitive electrode is almost the same as the other capacitive electrode with a different biomass as shown in Table 5.

The energy density and power density of the ACC-900 sample was calculated using standard equations. The energy density and power density for ACC-900 are 6.4 W h Kg<sup>-1</sup> and 46.17 W Kg<sup>-1</sup> respectively. These values are similar to the energy and power density of electrodes produced from biomass materials such as tobacco waste [30] and Dead Ginkgo Leaves [31]. The carbon electrodes produced from tobacco biomass produce an energy density and power density of 2.66 W h Kg<sup>-1</sup> and 52 W Kg<sup>-1</sup> while Dead Ginkgo Leaves produce an energy density and power density of 9.2 W h Kg<sup>-1</sup> and 48 W Kg<sup>-1</sup> respectively.

#### 4. CONCLUSION

Coconut husk based activated carbon has excellent physical and electrochemical properties required for supercapacitor electrode. The crystallinity of the carbon sample showed the presence of an amorphous carbon. The findings in this study revealed that the activation temperature of 900°C resulted in a decrease in the diameter of nanofibers, increase in carbon content, decrease in density, improved properties of porosity and surface area of the samples, improved physical and capacitive properties and increase in the purity of the carbon electrodes for supercapacitor application. Thus, the activation temperature of 900 °C is the best temperature for producing coconut husk based activated carbon electrodes for supercapacitor application.

#### ACKNOWLEDGMENTS

The author would like to thank the DRPM Kemenristek-Dikti through the second year Project of PDUPT with the title “Potential of Urban Solid Waste Utilization as a Supercapacitor Electrode” with contract number: 360/UN.19.5.1.3/PP/2018. The author also thanks the DRPM for the research funding by HIBAH KOMPETENSI the third year (2017) with the project title “Biomass-Based Nano

Carbon as Core Electrode for Supercapacitor Application” with contract number: 539/UN/19.5.1.3/PP/2017.

## References

1. Databox, 2017. Indonesia, Negara Produsen Kelapa Terbesar di Dunia. <https://databoks.katadata.co.id/datapublish/2017/01/06/indonesia-negara-produsen-kelapa-terbesar-di-dunia> (accessed 12 July 2018).
2. E. V. Anoop, V. V. Sheena, P. Aruna, V. Ajayghosh, *J. Indian Acad. Wood Sci.*, 8(2011) 76.
3. T. Logeswaran, G. P. Karthikeyan, M. Dinesh, B. Irbanaparvin, *Int. J. Adv. Research in Electrical, Electronics and Instrumentation Engineering*, 6 (2017) 1109.
4. E. Budi, *J. penelitian sains*, 14 (2011) 14406-25.
5. D. A. Nugroho, P. Aji, *Agriculture and Agricultural Science Procedia*, 3 (2015) 278.
6. M. Ali, N. Chouw, *Construction and Building Materials*, 41 (2013) 681.
7. A. Divyashree, S. A. Bt. A. Manaf, S. Yallappa, K. Chaitra, N. Kathyayini, G. Hegde, *J. Energy Chemistry*, 25(2016) 880.
8. M. Zhang, Y. Li, H. Si, B. Wang and T. Song, *Int. J. Electrochem. Sci.*, 12 (2017) 7844.
9. E. Taer, W. S. Mustika, Agustino, Fajarini, N. Hidayu and R. Taslim, *IOP Conf. Series: Earth and Environmental Science*, 58 (2017) 012065.
10. L. Yin, Y. Chen, D. Li, X. Zhao, B. Hou, B. Cao, *Materials and Design*, 111 (2016) 44.
11. E. Taer, M. Deraman, I. A. Talib, A. Awitdrus, S. A. Hashmi, A. A. Umar, *Int. J. Electrochem. Sci.*, 6 (2011) 3301.
12. R. Farma, M. Deraman, R. Omar, Awitdrus, M. M. Ishak, E. Taer, I. A. Talib, *AIP Conf. Proc.*, 1415 (2011) 180.
13. E. Taer, Apriwandi, Yusriwandi, W. S. Mustika, Zulkifli, R. Taslim, Sugianto, B. Kurniasih, Agustino, P. Dewi, *AIP Conf. Proc.*, 1927 (2018) 030036-1.
14. M. Deraman, R. Daik, S. Soltaninejad, N. S. M. Nor, Awitdrus, R. Farma, N. F. Mamat, N. H. Basri, M. A. R. Othman, *Adv. Materials Research*, 1108 (2015) 1.
15. Iwantono, E. Taer, A. A. Umar; Optimization Growth of Platinum and Palladium Nanoparticles on Stainless Steel 316L and Activated Carbon Pellet Substrates; *AIP Conf. Proc.*, 1454 (2012) 251.
16. E. Taer, Sugianto, M. A. Sumantre, R. Taslim, Iwantono, D. Dahlan, M. Deraman, *Adv. Materials Research*, 896 (2014) 66.
17. S. Hayashi, A. P. Mc Mahon, *Developmental Biology*, 244 (2002) 305.
18. G. Leofanti, M. Padovan, G. Tozzola, B. Venturelli, *Catal. Today*, 41 (1998) 219.
19. E. Taer, H. Yusra, Iwantono, R. Taslim, *J. Fisika dan Aplikasinya*, 1 (2016) 45.
20. M. Brebu, C. Vasile, *Cellulose Chem. Technol.*, 44 (2010) 353.
21. A. Tsamba, W. Yang, *Fuel Process Technol.*, 87 (2006) 523.
22. F. Li, W. Chi, Z. Shen, Y. Wu, Y. Liu, H. Liu, *Fuel Process Technol.*, 91 (2010) 17.
23. P. J. M. Carrott, J. M. V. Nabais, M. M. L. R. Carrott, J. A. Pajares, *Carbon*, 39 (2001) 1543.
24. B. D. Cullity; *Elements of X-Ray Diffraction*, Ed. 3 (2001), Amazon Prentice Hall.
25. Awitdrus, M. Deraman, I. A. Talib, R. Omar, M. H. Jumali, E. Taer, M. H. Saman, *Sains Malaysiana*, 39 (2010) 83.
26. J. M. V. Nabais, J. G. Teixeira, I. Almeida, *Bioresource Technol.*, 102 (2010) 2781.
27. K. Kumar, R. K. Saxena, R. D. Kothari, K. Suri, N. K. Kaushik, J. N. Bohra, *Carbon*, 35 (1997) 1842.
28. M. Inagaki, H. Konno, O. Tanaike, *J. Power Sources*, 195 (2010) 7880.
29. E. Taer, Zulkifli, Sugianto, R. Taslim, *Prosiding Seminar Nasional Fisika*, (2015) 05.
30. H. Chen, Y-C. Guo, F. Wang, G. Wang, P-R.Qi, X-H. Guo, B. Dai, F. Yu, *New Carbon Materials*, 32 (2017) 592.

31. X. Zhu, S. Yu, K. Xu, Y. Zhang, L. Zhang, G. Lou, Y. Wu, E. Zhu, H. Chen, Z. Shen, B. Bao, S. Fu, *Chemical Engineering Science*, 181 (2018) 36.
32. H. Wang, Z. Xu, A. Kohandehghan, Z. Li, K. Cui, X. Tan, T. J. Stephenson, C. K. King'andu, C. M. B. Holt, B. C. Olsen, J. K. Tak, D. Harfield, A. O. Anyia, D. Mitlin, *Acs nano*, 7 (2013) 5131.
33. L. Deng, W. Zhong, J. Wang, P. Zhang, H. Fang, L. Yao, X. Liu, X. Ren, Y. Li, *Electrocim. Acta*, 228 (2017) 398.
34. J. Cai, H. Niu, H. Wang, H. Shao, J. Fang, J. He, H. Xiong, C. Ma, T. Lin, *J. Power Sources*, 324 (2016) 302.
35. Y. Zhang, F. Wang, H. Zhu, L. Zhou, X. Zheng, X. Li, Z. Chen, Y. Wang, D. Zhang, D. Pan, *Applied Surface Science*, 426 (2017) 99.
36. L. K. Ong, A. Kurniawan, A. C. Suwandi, C. X. Lin, X. S. Zhao, S. Ismadji, *Progress in Natural Science: Materials International*, 22 (2012) 624.
37. E. Taer, Y. Susanti, Awitdrus, Sugianto, R. Taslim, R. N. Setiadi, S. Bahri, Agustino, P. Dewi, B. Kurniasih, *AIP Conference Proceedings*, 1927 (2018) 030016,
38. Y. Lv, L. Gan, M. Liu, W. Xiong, Z. Xu, D. Zhu, D. S. Wright, *J. Power Sources*, 209 (2012) 152.
39. R. Farma, M. Deraman, A. Awitdrus, I. A. Talib, E. Taer, J. G. Manjunatha, M. M. Ishak, B. N. M. Dollah, S. A. Hashmi, N. H. Basri, *Bioresource Technol.*, 132 (2013) 254.
40. E. Taer, R. Taslim, W. S. Mustika, B. Kurniasih, Agustino, A. Afrianda, Apriwandi, *Int. J. Electrochem. Sci.*, 13 (2018) 8428.

© 2018 The Authors. Published by ESG ([www.electrochemsci.org](http://www.electrochemsci.org)). This article is an open access article distributed under the terms and conditions of the Creative Commons Attribution license (<http://creativecommons.org/licenses/by/4.0/>).